Polyhedron 151 (2018) 433–440

Contents lists available at ScienceDirect

Polyhedron

journal homepage: www.elsevier.com/locate/poly

Homometallic {Mn_{10}} and heterometallic {Mn_6Ca_4} supertetrahedra exhibiting an unprecedented {$Mn^{III}_9Mn^{II}$} oxidation state level and heterometal ions distribution

Katerina Skordi [a], Constantina Papatriantafyllopoulou [a,b,c], Sotiris Zartilas [a], Katye M. Poole [b], Vassilios Nastopoulos [d], George Christou [b], Anastasios J. Tasiopoulos [a,*]

[a] Department of Chemistry, University of Cyprus, 1678 Nicosia, Cyprus
[b] Department of Chemistry, University of Florida, Gainesville, FL 32611, United States
[c] School of Chemistry, National University of Ireland Galway, Galway, Ireland
[d] Department of Chemistry, University of Patras, 26504 Patras, Greece

ARTICLE INFO

Article history:
Received 28 March 2018
Accepted 12 May 2018
Available online 22 May 2018

Dedicated to Professor Spyros P. Perlepes, the great teacher, valuable collaborator and dear friend, for his contribution on the development of Inorganic Chemistry in Greece on the occasion of his 65th birthday.

Keywords:
Manganese clusters
Polyols
Crystal structures
Magnetic properties
Ferromagnetic exchange interactions

ABSTRACT

Two novel decametallic clusters displaying a supertetrahedral structural core are discussed, a homometallic compound $[Mn^{III}_9Mn^{II}(\mu_4\text{-}O)_4(\mu_3\text{-}OMe)_3(btH)_3(ed)_3(PhCO_2)_6]\cdot 6H_2O$ (**1**·$6H_2O$) (btH_3 = (±)-1,2,4-butanetriol; edH_2 = 1,2-ethanediol) and a heterometallic one $[Mn^{III}_6Ca^{II}_4(\mu_4\text{-}O)_4(\mu_3\text{-}Cl)_4(pd)_6Cl_2(MeOH)_{10}]$ (**2**) (pdH_2 = 1,3-propanediol). In particular complex **1**·$6H_2O$ is a new member of an extended family of homometallic Mn_{10} supertetrahedra which exhibits an unprecedented $Mn^{III}_9Mn^{II}$ oxidation state level. It is based on a supertetrahedral $[Mn^{III}_9Mn^{II}(\mu_4\text{-}O)_4]^{21+}$ core with its peripheral ligation being completed by bridging alkoxy (OMe^-, btH^{2-}, ed^{2-}) and carboxylate ($PhCO_2^-$) ligands. Complex **2** is a unique heterometallic analogue of the family of complexes displaying the well-known $[Mn^{III}_6Mn^{II}_4(\mu_4\text{-}O)_4]^{18+}$ supertetrahedral core in which the Mn^{II} ions have been replaced by Ca^{II} ions. The peripheral ligation of the heterometallic $[Mn^{III}_6Ca^{II}_4(\mu_4\text{-}O)_4]^{18+}$ core is completed by both bridging (μ_3-Cl^- and pd) and terminal (Cl^-, MeOH) ligands. Magnetism studies revealed that complex **1**·$6H_2O$ displays dominant ferromagnetic exchange interactions and a large spin ground state value S_T = 23/2 whereas complex **2** exhibits exclusively ferromagnetic exchange interactions and the maximum possible spin ground state S_T = 12 for a complex consisting of six Mn^{III} and four Ca^{II} ions.

© 2018 Elsevier Ltd. All rights reserved.

1. Introduction

Polynuclear clusters of paramagnetic 3d metal ions have attracted intense interest in the last two decades for a number of reasons including their novel crystal structures and magnetic properties [1–4]. Such compounds often exhibit impressive crystal structures with unique features such as high nuclearities and aesthetically pleasing, high symmetry structural cores [1]. In addition they sometimes display interesting magnetic properties including the presence of ferromagnetic exchange interactions that lead to large or even abnormally large spin ground state values [2–7]. The construction of molecular aggregates possessing large S_T values has been a challenge for synthetic chemists since they are related to interesting phenomena and hot research areas such as single molecule magnetism [2–4] and magnetic refrigeration [8].

The most successful synthetic methods towards metal clusters exhibiting large S_T values include the use of ligands that usually lead to ferromagnetic exchange interactions [9] or the employment of ligands and synthetic procedures that lead to complexes that are known to display ferromagnetic exchange interactions [10]. One family of compounds that has attracted intense interest because of their high symmetry structural core and the fact that they usually exhibit entirely ferromagnetic exchange interactions are those containing the decametallic supertetrahedral core. A Cambridge database search for decametallic discrete Mn complexes exhibiting the $[Mn_{10}(\mu_4\text{-}O)_4]^{n+}$ supertetrahedral core gave twelve hits and a second one for all compounds containing this core even as fragment of high nuclearity clusters or as fragment or repeating unit of multidimensional coordination polymers returned over thirty hits [6,7,11–26]. The extended appearance of this core in Mn carboxylate chemistry reveals not only its significance for this area but also its ability to be stabilized with a series of chelating ligands. The most widely appeared ligands in decametallic

* Corresponding author. Fax: +357 22895451.
E-mail address: atasio@ucy.ac.cy (A.J. Tasiopoulos).

https://doi.org/10.1016/j.poly.2018.05.029
0277-5387/© 2018 Elsevier Ltd. All rights reserved.

supertetrahedral compounds are various aminoalcohols [11–14], diols [7,16,17,19,20,22–26] and triols [6,17], although such compounds have been stabilized with a variety of ligands including oxacalix[3]arene [18], benzotriazole [21], etc. Intense interest has attracted the most commonly appeared $[Mn^{III}_6Mn^{II}_4(\mu_4\text{-}O)_4]^{18+}$ supertetrahedral core since it usually displays entirely ferromagnetic exchange interactions and the maximum possible spin ground state value $S_T = 22$. Interestingly, members of this family displayed enhanced magnetocaloric effect and were proposed for use in magnetic refrigeration applications [11,12]. In addition, this core has appeared as fragment in high nuclearity $[Mn_{17}]$ [7] and $[Mn_{19}]$ [6] clusters which consist of two edge- or vertex-sharing $[Mn^{III}_6Mn^{II}_4(\mu_4\text{-}O)_4]^{18+}$ sub-units respectively. The exchange interactions within these clusters are entirely ferromagnetic resulting in giant S_T values of 37 ($[Mn_{17}]$) and 83/2 ($[Mn_{19}]$) which correspond to the highest S_T value reported for a SMM and the second highest S_T value for any metal cluster in general, respectively. Furthermore, this core also has appeared as fragment in nanosized homometallic and heterometallic aggregates including the giant $[Mn_{49}]$ cuboctahedron consisting of eight tightly connected $[Mn^{III}_6Mn^{II}_4(\mu_4\text{-}O)_4]^{18+}$ supertetrahedral sub-units [24] and a $[Mn_{36}Ni_4]$ 'loop-of-loops-and-supertetrahedra' complex [25] consisting of two $[Mn^{III}_8Ni^{II}_2]$ loops and two $[Mn^{III}_6Mn^{II}_4(\mu_4\text{-}O)_4]^{18+}$ supertetrahedra. These compounds display dominant ferromagnetic exchange interactions leading to large S_T values (61/2 in the case of $[Mn_{49}]$ aggregate and 26 in the case of $[Mn_{36}Ni_4]$ compound). The presence of decametallic supertetrahedra in the repeating units of multidimensional coordination polymers has also been realized with the list of such species containing compounds based on a $[Mn^{III}_6Mn^{II}_4(\mu_4\text{-}O)_4]^{18+}$ and a $[Mn^{III}_{11}Mn^{II}_6(\mu_4\text{-}O)_8]^{29+}$ repeating units [7,16,23]. Apart from the rather common $[Mn^{III}_6Mn^{II}_4]$ oxidation state level, the decametallic supertetrahedral core has also appeared at the $[Mn^{III}_4Mn^{II}_6]$ [18–20] and $[Mn^{III}_{10}]$ [21] ones. In addition, the heterometallic $[Mn_{10-x}M_x(\mu_4\text{-}O)_4]^{n+}$ (M = any metal ion) supertetrahedral core, has also appeared only once in discrete form in a $Mn^{III}_4Ce^{IV}_6$ cluster [27]. It has also been observed a few times as a fragment in high nuclearity $[Mn^{III}_9Dy^{III}_8]$ [28] and $[Mn^{III}_{12}Mn^{II}_6M]$ (M = Dy^{III}, Y^{III}, Lu^{III}, Sr^{II} and Cd^{II}) [29,30] aggregates consisting of two edge- or vertex-sharing decametallic supertetrahedra, respectively and in the nanosized $[Mn_{25}Na_4]$ aggregate containing four edge-sharing $[Mn^{III}_6Mn^{II}_3Na^{I}]$ supertetrahedral repeating units [24].

Herein we report the synthesis, structural, spectroscopic and magnetic characterization of two new compounds, a homometallic $[Mn^{III}_9Mn^{II}(\mu_4\text{-}O)_4(\mu_3\text{-}OMe)_3(btH)_3(ed)_3(PhCO_2)_6]\cdot 6H_2O$ (**1**·$6H_2O$) (btH_3 = (±)-1,2,4-butanetriol; edH_2 = 1,2-ethanediol) and a heterometallic $[Mn^{III}_6Ca^{II}_4(\mu_4\text{-}O)_4(\mu_3\text{-}Cl)_4(pd)_6Cl_2(MeOH)_{10}]$ (**2**) (pdH_2 = 1,3-propanediol) one, exhibiting supertetrahedral structural cores. Complex **1** displays an unprecedented in the rich family of Mn-based decametallic supertetrahedra $[Mn^{III}_9Mn^{II}]$ oxidation state level whereas complex **2** is a unique heterometallic analogue of the family of complexes containing the $[Mn^{III}_6Mn^{II}_4(\mu_4\text{-}O)_4]^{18+}$ core in which the Mn^{II} ions are replaced by Ca^{II} ions. Magnetism studies revealed the presence of dominant ferromagnetic exchange interactions in **1**·$6H_2O$ leading to large S_T = 23/2 and entirely ferromagnetic exchange interactions in **2** affording an S_T = 12.

2. Experimental

2.1. General and physical measurements

All manipulations were performed under aerobic conditions using materials (reagent grade) and solvents as received. $[Mn_3O(O_2CPh)_6(py)_2(H_2O)]$ was prepared as described elsewhere [31].

Microanalyses (C, H, N) were performed by the in-house facilities of the University of Cyprus, Chemistry Department. IR spectra (4000–400 cm^{-1}) were recorded on a Shimadzu Prestige-21 spectrometer with the samples prepared as KBr pellets. Variable-temperature dc and ac magnetic susceptibility data were collected at the University of Florida using a Quantum Design MPMS-XL SQUID susceptometer equipped with a 7 T magnet and operating in the 1.8–300 K range. Samples were embedded in solid eicosane to prevent torquing. The ac magnetic susceptibility measurements were performed in an oscillating ac field of 3.5 G and a zero dc field. Pascal's constants were used to estimate the diamagnetic corrections, which were subtracted from the experimental susceptibilities to give the molar paramagnetic susceptibility (χ_M).

2.2. Compound preparation

2.2.1. $[Mn^{III}_9Mn^{II}(\mu_4\text{-}O)_4(\mu_3\text{-}OMe)_3(btH)_3(ed)_3(PhCO_2)_6]\cdot 6H_2O$ (**1**·$6H_2O$)

A colorless solution of btH_3 (0.095 ml, 0.11 g, 1.06 mmol) in MeOH (5 ml) was added to a brown solution of $[Mn_3O(O_2CPh)_6(py)_2(H_2O)]$ (0.20 g, 0.18 mmol) in MeOH (10 ml) and to the resulting brown slurry was added solid NaOCN (0.047 g, 0.72 mmol). The reaction mixture was left under magnetic stirring for 40 min and the resulting solution remained undisturbed for 15 min. Then it was filtered off and the filtrate was left to slowly evaporate at room temperature. After a few weeks X-ray quality crystals of **1**·$3H_2O$ were formed. The reaction yield was 20% based on total Mn content. The dried solid was analyzed as **1**·$6H_2O$. *Anal.* Calc.: C, 37.21; H, 4.31. Found: C, 36.92; H, 4.38. IR (KBr, cm^{-1}): 3119b, 2848w, 1638 s, 1618 s, 1570 m, 1400 s, 1105 m, 1036 m, 947w, 777w, 718 m, 679 m, 625 m, 561 m, 480 m.

2.2.2. $[Mn^{III}_6Ca^{II}_4(\mu_4\text{-}O)_4(\mu_3\text{-}Cl)_4(pd)_6Cl_2(MeOH)_{10}]$ (**2**)

pdH_2 (0.15 ml, 0.16 g, 2.1 mmol), NEt_3 (0.14 ml, 0.10 g, 1.0 mmol) and solid $CaCl_2 4H_2O$ (0.09 g, 0.5 mmol) were added to a solution of $MnCl_2\cdot 4H_2O$ (0.10 g, 0.5 mmol) in MeCN/MeOH (25/4 ml). The resulting orange slurry was gently heated for 1 h under stirring during which time it turned to a brown solution. The latter was filtered off and the filtrate left to stand undisturbed in a closed flask. After five days, X-ray quality, orange, rod-shaped crystals of **2** were observed. The crystals were collected by filtration, washed with cold MeCN and dried on air. The reaction yield was 40% based on total Mn content. The dried solid analyzed satisfactorily as **2**. *Anal.* Calc.: C, 21.96; H, 5.00. Found: C, 21.68; H, 5.21. IR (KBr, cm^{-1}): 3218b, 2915w, 2882w, 1564 s, 1522 m, 1481 s, 1475 s, 1304 m, 1269 m, 1253w, 1224 m, 1196 m, 1123 m, 1129 m, 1097 s, 1063 s, 980 m, 922 m, 910 s, 883w, 809 m, 780 m, 751 m, 732 m, 624 m, 590 m.

2.3. Single-crystal X-ray crystallography

Data were collected on a SuperNova A Oxford Diffraction diffractometer, equipped with a CCD area detector and a graphite monochromator utilizing Cu-Kα (λ = 1.54184 Å) and Mo Kα radiation (λ = 0.71073 Å) for **1**·$3H_2O$ and **2**, respectively. Suitable crystals covered with paratone-N oil were mounted on the tip of glass fibers or scooped up in cryo-loops at the end of a copper pin and transferred to a goniostat where they were cooled for data collection. Empirical absorption corrections (multi-scan based on symmetry-related measurements) were applied using CRYSALIS RED software [32]. The structures were solved by direct methods with SIR92 [33] and refined on F^2 using full-matrix least squares with SHELXL97 [34]. The program SQUEEZE [35], a part of the PLATON package of crystallographic software, was used to remove contribution of highly disordered solvent molecules in **1**·$3H_2O$. Software packages used: CrysAlis CCD for data collection [32], CrysAlis RED for cell refinement and data reduction [32], WINGX for geometric calculations [36], and DIAMOND [37] for molecular graphics. The non-H

Table 1
Crystallographic data for complexes **1**·3H_2O and **2**.

Complex	**1**·3H_2O	**2**
Empirical formula	$C_{63}H_{72}Mn_{10}O_{37}$	$C_{28}H_{54}Ca_4Cl_6Mn_6O_{26}$
Formula weight	1970.03	1509.37
Crystal system	cubic	monoclinic
Space group	$Pa\bar{3}$	$C2/c$
Unit cell dimensions		
a (Å)	25.6527(2)	18.7571(8)
b (Å)	25.6527(2)	15.4398(7)
c (Å)	25.6527(2)	21.092(2)
β (°)		98.772(2)
V (Å^3)	16881.0(2)	6036.9(5)
Z	8	4
ρ (g cm^{-3})	1.550	1.661
λ (Å)	1.54184	0.71073
μ (mm^{-1})	12.462	1.892
T (K)	100(2)	100(2)
Measured/independent reflections (R_{int})	54478/4385 (0.0666)	14018/5322 (0.0371)
Obsd reflections [$I > 2\sigma(I)$]	2729	4484
Parameters refined	331	326
GoF (on F^2)	1.018	0.940
R_1[a] ($I > 2\sigma(I)$)	0.0596	0.0459
wR_2[b] ($I > 2\sigma(I)$)	0.1877	0.1316
$(\Delta\rho)_{maximum}/(\Delta\rho)_{minimum}$ (e Å^{-3})	1.230/−0.483	1.860/−1.200

[a] $R_1 = \Sigma(||F_o| - |F_c||)/\Sigma(|F_o|)$.
[b] $wR_2 = \{\Sigma[w(F_o^2 - F_c^2)^2]/\Sigma[w(F_o^2)^2]\}^{1/2}$.

atoms were treated anisotropically, whereas the hydrogen atoms were placed in calculated, ideal positions and refined as riding on their respective carbon atoms. In compound **1**, the H atoms of the alcohol O atom of the organic ligand btH^{2-} and these of the H_2O solvent molecules could not be located. The H atoms of one independent pd^{2-} ligand (totally two in the molecule) and the alcohol O atom of terminal MeOH molecules could not be located in the molecule of **2**. Unit cell data and structure refinement details for compounds **1**·3H_2O and **2** are listed in Table 1. Full details can be found in the CIF files provided in Supplementary information.

3. Results and discussion

3.1. Synthesis

Our group has been investigating the use of polyols in Mn carboxylate chemistry. These investigations have focused on the use of diols and especially of 1,3-propanediol (pdH_2) and its derivatives as a strategy for the synthesis of high nuclearity Mn clusters exhibiting interesting magnetic properties [7,10,23–26]. These ligands have been shown to stabilize complexes containing the $[Mn^{III}_6Mn^{II}_4(\mu_4\text{-}O)_4]^{18+}$ core either in a discrete form or as fragment of high nuclearity clusters [7,16,17,22–26]. These investigations have been recently extended towards various directions. These include the use in Mn carboxylate chemistry of various triols that have not been widely employed in metal cluster chemistry. Thus, the use of 3-methyl-1,3,5-pentanetriol ($mptH_3$) in Mn carboxylate chemistry afforded a $[Mn^{II}_6Mn^{III}_6]$ single – strand molecular wheel with a reuleaux triangular topology [38] and a $[Mn^{III}_{13}Mn^{IV}_2]$ 3 × 5 molecular grid [39]. Further investigations in this area included the use of the aliphatic triol btH_3. To the best of our knowledge there are no metal clusters reported in the literature containing this ligand. Thus, the reaction of $[Mn_3O(O_2CPh)_6(py)_2(H_2O)]$ with btH_3 in the presence of NaOCN in ~1:6:4 molar ratio in MeOH afforded a brown solution which was left undisturbed to slowly evaporate at room temperature for a few weeks, upon which brown X-ray quality crystals of **1**·3H_2O were formed in 20% yield; the dried solid was analyzed as **1**·6H_2O. The NaOCN salt, although neither its cation nor its anion appear in **1**, is essential for the formation of the metal cluster since reactions performed in its absence led to microcrystalline products that we were unable to further characterize. Note that despite the fact that edH_2 ligand was added in the reaction mixture as one of the coexisting polyols contained as impurities in commercially available btH_3, the synthesis of **1**·6H_2O is highly reproducible. The formation of complex **1** is summarized in Eq. (1).

$$10[Mn^{III}_2Mn^{II}O(O_2CPh)_6(py)_2(H_2O)] + 9btH_3 + 9edH_2 + 9MeOH + 1.75O_2 + 6,5H_2O \xrightarrow{MeOH} 3[Mn^{III}_9Mn^{II}(\mu_4\text{-}O)_4(\mu_3\text{-}OMe)_3\text{-}(btH)_3(ed)_3(PhCO_2)_6]\cdot 6H_2O + 20py + 42PhCO_2H \quad (1)$$

A second extension of our research programme on the use of polyols in Mn carboxylate chemistry involved the use of paramagnetic or diamagnetic heterometals targeting to mixed metal compounds. Particular attention has attracted the use of diamagnetic heterometals in Mn/pdH_2 reactions especially after the discovery of a 3-D coordination polymer based on a high-spin $[Mn_{19}Na]$ repeating unit [40]. These investigations have afforded some high nuclearity clusters displaying aesthetically pleasing crystal structures and interesting magnetic properties such as a nanosized $[Mn_{40}Na_4]$ 'loop-of-loops' aggregate consisting of four $[Mn^{III}_8Mn^{II}_2Na^{I}]$ loops [41] and a $[Mn_{15}K]$ loop incorporating a supertetrahedron [26]. These studies were also extended to the use of Ca^{II} salts in Mn/pdH_2 chemistry targeting to mixed Mn^{n+}/Ca^{II} clusters. Such compounds have attracted attention not only for their interesting magnetic properties and crystal structures but also because they could possibly serve as structural models of the Mn_4Ca cluster appearing in the active site of photosystem II that is responsible for the photocatalytic oxidation of H_2O to O_2 [42]. In fact, compound **2** is the initial result of these studies. Thus, the reaction of $MnCl_2\cdot 4H_2O$ and $CaCl_2 4H_2O$ with pdH_2 in the presence of NEt_3 in ~1:1:4:2 molar ratio in MeCN/MeOH (25/4 ml) afforded a brown solution which was left undisturbed in a closed flask for five days, upon which orange X-ray quality crystals of **2** were formed in 40% yield; the dried solid was analyzed as solvent free **2**.

The formation of complex **2** is summarized in Eq. (2).

$$6MnCl_2\cdot 4H_2O + 4CaCl_2\cdot 4H_2O + 6pdH_2 + 10MeOH + 1.5O_2 \xrightarrow{MeCN/MeOH} [Mn^{III}_6Ca^{II}_4(\mu_4\text{-}O)_4(\mu_3\text{-}Cl)_4(pd)_6Cl_2(MeOH)_{10}] + 14HCl + 39H_2O \quad (2)$$

3.2. Description of structures

Representations of the molecular structure and the structural core of compound **1** are shown in Fig. 1 and selected interatomic distances and angles are listed in Table S1.

Complex **1**·3H_2O (Fig. 1) crystallizes in the cubic space group $Pa\bar{3}$ and its asymmetric unit consists of one third of the Mn_{10} cluster and one crystallization water molecule. Its metallic skeleton consists of a mixed valent $Mn^{III}_9Mn^{II}$ supertetrahedron in which the Mn^{II} ion occupies one of the apex positions. The oxidation states of the Mn ions [43] and the protonation levels of the O atoms [44] were determined by bond valence sum (BVS) calculations, charge considerations and inspection of metric parameters. All Mn^{III} ions are hexacoordinated, displaying a distorted octahedral coordination geometry and containing the expected, for high spin d^4 ions, Jahn–Teller (JT) elongations (the JT axes are not co-parallel). The Mn^{II} ion is heptacoordinated although one of the bond lengths is too long (Mn4···O8 = 2.567(8) Å) and thus this interaction can only be marginally considered as a covalent bond. The metal ions are connected by four $\mu_4\text{-}O^{2-}$ ions forming the $[Mn^{III}_9Mn^{II}(\mu_4\text{-}O)_4]^{21+}$ core which consists of three $[Mn^{III}_4(\mu_4\text{-}O)]^{10+}$ and one $[Mn^{III}_3Mn^{II}(\mu_4\text{-}O)]^{9+}$ vertex-sharing tetrahedra. The Mn ions of the $[Mn^{III}_4(\mu_4\text{-}O)]^{10+}$ tetrahedra are connected through two $PhCO_2^-$ ions bridging one pair of

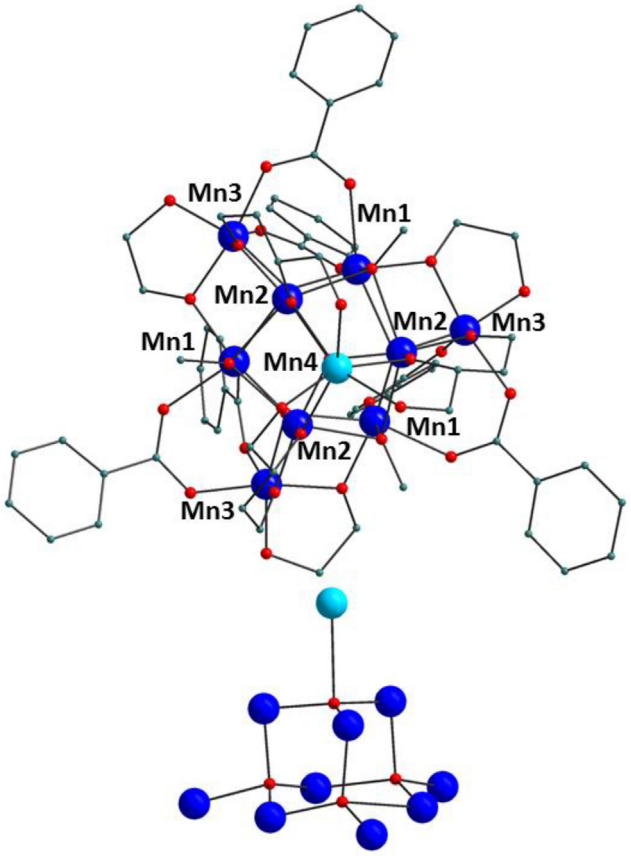

Fig. 1. Partially labeled representation of the molecular structure of complex **1** (top) and its $[Mn_9^{III}Mn^{II}(\mu_4\text{-}O)_4]^{21+}$ supertetrahedral structural core (bottom). Colour code: Mn^{III}, blue; Mn^{II}, cyan; O, red; C, grey. The hydrogen atoms are omitted for clarity. (Colour online.)

Mn ions in a *syn,syn*-$\eta^1{:}\eta^1{:}\mu$ coordination mode and through a $\eta^2{:}\eta^1{:}\mu$ ed^{2-} ligand bridging another pair of Mn ions. The three $[Mn_4^{III}(\mu_4\text{-}O)]^{10+}$ tetrahedra are held together by three μ_3-OMe bridges. The Mn ions of the $[Mn_3^{III}Mn^{II}(\mu_4\text{-}O)]^{9+}$ tetrahedron are connected through three $\eta^2{:}\eta^2{:}\eta^1{:}\mu_3$ btH^{2-} ligands occupying six of the coordination sites of the Mn^{II} ion and connecting it to the other Mn ions of the same tetrahedron and also to Mn ions of the $[Mn_4^{III}(\mu_4\text{-}O)]^{10+}$ tetrahedra.

Complex **1** is a new member of the extended family of the decametallic supertetrahedra possessing a $[Mn_{10}(\mu_4\text{-}O)_4]^{n+}$ core. In the past several clusters displaying a decametallic supertetrahedral core either in a discrete form or as part of a high nuclearity cluster or repeating unit of a coordination polymer had been reported with various chelating ligands. These complexes exhibited the oxidation state levels $[Mn_4^{III}Mn_6^{II}]$ [18–20], $[Mn_6^{III}Mn_4^{II}]$ [6,7,11–17,22–25] and $[Mn_{10}^{III}]$ [21] (Fig. 2) with the $[Mn_6^{III}Mn_4^{II}]$ one being by far the most common oxidation state level shown in decametallic supertetrahedra. Interestingly, the $[Mn_9^{III}Mn^{II}]$ oxidation state distribution appeared in **1** is observed for the first time in this family of $[Mn_{10}]$ supertetrahedra.

Representations of the molecular structure and the structural core of compound **2** are shown in Fig. 3 and selected interatomic distances and angles are listed in Table S2.

Complex **2** (Fig. 3) crystallizes in the monoclinic space group *C*2/*c* and its asymmetric unit consists of half of the $[Mn_6^{III}Ca_4^{II}]$ cluster. The metallic skeleton of **2** consists of a heterometallic $Mn_6^{III}Ca_4^{II}$ supertetrahedron in which the Ca^{II} ions occupy the apex positions. The oxidation states of the Mn ions [43] and the protonation levels of the O atoms [44] were determined by bond valence sum (BVS) calculations, charge considerations and inspection of metric parameters. All Mn^{III} ions are hexacoordinated, displaying a distorted octahedral coordination geometry and containing the expected, for high spin d^4 ions, JT elongation axes which are not co-parallel. The Ca^{II} ions are either hexacoordinated (Ca1) or heptacoordinated (Ca2). The Ca^{II} ions occupy the apex positions of a tetrahedron and the Mn^{III} ones are located in its edges. The metal ions are connected by four μ_4-O^{2-} ions forming the $[Mn_6^{III}Ca_4^{II}(\mu_4\text{-}O)_4]^{18+}$ core (Fig. 3) which consists of four $[Mn_3^{III}Ca^{II}(\mu_4\text{-}O)]^{9+}$ vertex-sharing tetrahedra. In fact, the $[Mn_6^{III}Ca_4^{II}(\mu_4\text{-}O)_4]^{18+}$ core is analogous to the commonly appeared homometallic $[Mn_6^{III}Mn_4^{II}(\mu_4\text{-}O)_4]^{18+}$ supertetrahedral core in which the Mn^{II} ions have been replaced by Ca^{II} ions. The Mn^{III} ions are bridged through four μ_3-Cl^- ions which occupy their JT axes. The two Ca^{II} and one Mn^{III} ions located in each edge of the tetrahedron are connected through one pd^{2-} ligand (totally 6 pd^{2-} in **2**) bridging in a $\eta^2{:}\eta^2{:}\mu_3$ mode. The peripheral ligation of the Ca^{II} ions is completed by two terminal Cl^- ions and ten MeOH molecules. Alternatively the $[Mn_6^{III}Ca_4^{II}(\mu_4\text{-}O)_4]^{18+}$ core can be described as exhibiting an 'octahedron subscribed in a tetrahedron' metal topology (Fig. 3, bottom right). The inner octahedral unit is formed by the six Mn^{III} ions bridged through the four μ_3-Cl^- ions whereas the outer tetrahedral unit comprises the four Ca^{II} ions. The $[Mn_6^{III}(\mu_3\text{-}Cl)_4]^{14+}$ and $[Ca_4^{II}]$ sub-units are connected through the four μ_4-O^{2-} ions with each of them bridging three Mn^{III} and one Ca^{II} ions.

Complex **2** represents a rare example of a heterometallic $[Mn_{10-x}M_x]$ supertetrahedron. In fact, there have been only three types of mixed-metal supertetrahedra reported in the past, two of which appeared as fragments of high nuclearity clusters [24,27–30]. Their metallic skeletons are shown in Fig. 4 and compared to the one of complex **2**. To the best of our knowledge, there is only one other discrete heterometallic supertetrahedron, a $[Mn_4^{III}Ce_6^{IV}]$ aggregate [27]. In this compound the four Mn^{III} and the Ce^{IV} ions occupy the apices and the edges of the distorted supertetrahedron, respectively. The most common supertetrahedral unit, appeared as fragment of high nuclearity clusters, is the $[Mn_6^{III}Mn_3^{II}M]$ ($M = Na^+$, Sr^{2+}, Cd^{2+}, Y^{3+}, Dy^{3+}, Lu^{3+}) one in which the heterometal is located in one of the apex positions of the tetrahedron [24,29,30]. This unit has appeared in the $[Mn_{12}^{III}Mn_6^{II}M]$ ($M = Sr^{2+}$, Cd^{2+}, Y^{3+}, Dy^{3+}, Lu^{3+}) [29,30] aggregates consisting of two vertex-sharing

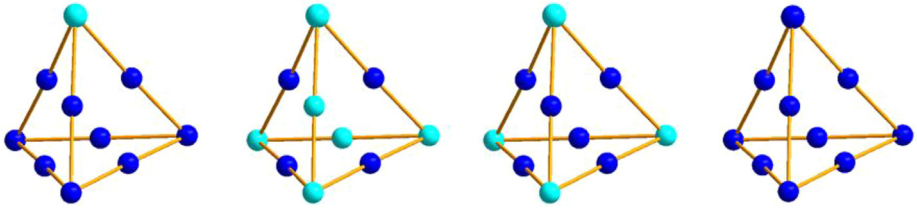

Fig. 2. The oxidation state distribution in complex **1** (left) and those of reported $[Mn_{10}]$ supertetrahedra.[6,7,11–25] From left to right the $[Mn_9^{III}Mn^{II}]$, $[Mn_4^{III}Mn_6^{II}]$, $[Mn_6^{III}Mn_4^{II}]$ and $[Mn_{10}^{III}]$ oxidation state distributions of decametallic supertetrahedra are shown. The solid lines connecting the metal ions are to emphasize the tetrahedral shape of the metallic skeletons. Colour code: Mn^{III}, blue; Mn^{II}, cyan. (Colour online.)

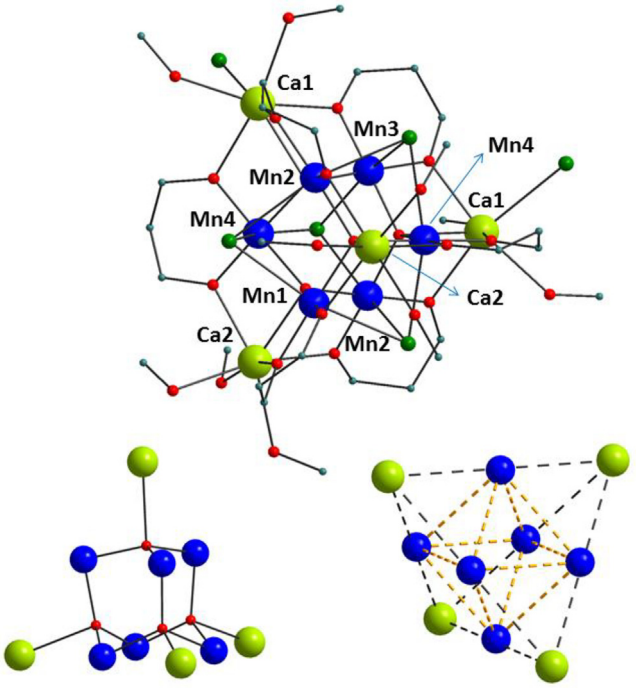

Fig. 3. Partially labeled representation of the molecular structure of complex **2** (top), its $[Mn^{III}_6Ca^{II}_4(\mu_4\text{-}O)_4]^{18+}$ supertetrahedral structural core (bottom, left) and the $[Mn^{III}_6Ca^{II}_4]$ metallic skeleton (bottom, right); the dashed lines connecting the metal ions in the bottom, right figure are to emphasize the description of the $[Mn^{III}_6Ca^{II}_4]$ metallic skeleton as a Mn^{III}_6 octahedron subscribed in a Ca^{II}_4 tetrahedron. Colour code: Mn^{III}, blue; Ca^{II}, light green; O, red; Cl, green; C, grey. The hydrogen atoms are omitted for clarity. (Colour online.)

$[Mn^{III}_6Mn^{II}_3M]$ supertetrahedra which are analogues of the high spin $S_T = 83/2$ $[Mn^{III}_{12}Mn^{II}_7]$ aggregate [6]. A similar $[Mn^{III}_6Mn^{II}_3M]$ (M = Na^+) core was also appeared recently as a repeating unit in a $[Mn_{25}Na_4]$ aggregate consisting of four such decametallic supertetrahedral units sharing their edges [24]. Finally a $[Mn^{III}_5Dy^{III}_5]$ supertetrahedral core appeared as fragment in a $[Mn^{III}_9Dy^{III}_8]$ aggregate composed of two supertetrahedral units sharing their edges [28]. From the above discussion and Fig. 4 it becomes apparent that complex **2** is a new type of heterometallic Mn-based supertetrahedron.

3.3. Magnetic properties

Solid-state dc magnetic susceptibility measurements were performed on polycrystalline samples of complexes **1**·6H_2O and **2**, under a magnetic field of 0.1 T in the temperature range 5–300 K. The obtained data are shown as $\chi_M T$ versus T plot in Fig. 5. For complex **1**·6H_2O, the $\chi_M T$ value increases slowly from 34.68 cm^3 mol^{-1} K at 300 K to 40.22 cm^3 mol^{-1} K at 100 K, then rapidly to

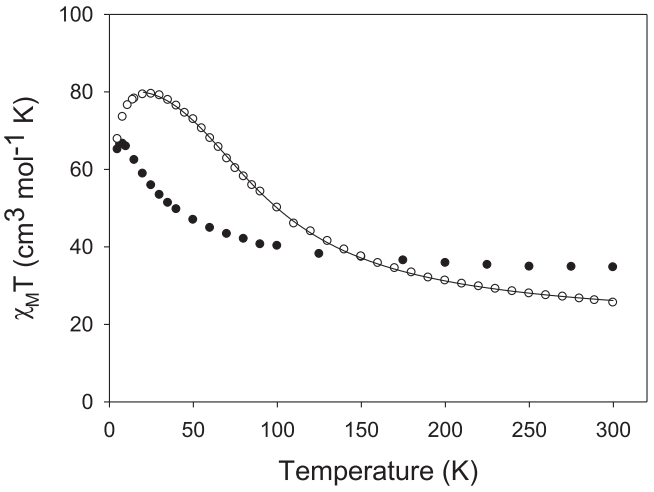

Fig. 5. $\chi_M T$ vs. T plots for complexes **1**·6H_2O (•) and **2** (○) in the temperature range 5–300 K in a 0.1 T applied dc field. The solid line is the fit of the data for **2**; see text for the fit parameters.

66.89 cm^3 mol^{-1} K at 10 K and decreases slightly to 65.11 cm^3 mol^{-1} K at 5 K. For **2**, the $\chi_M T$ value at 300 K is 25.55 cm^3 mol^{-1} K and increases continuously with decreasing temperature reaching to a near plateau value of ~79 cm^3 mol^{-1} K at 40–20 K and then decreases to 67.79 cm^3 mol^{-1} K at 5 K (Fig. 5). In both compounds the 300 K $\chi_M T$ value is higher than the corresponding spin-only ($g = 2$) values of 31.375 and 18 cm^3 mol^{-1} K expected for compounds consisting of 1 Mn^{II}/9 Mn^{III} (**1**·6H_2O) and six Mn^{III} (**2**) non-interacting ions, respectively. The shapes of the $\chi_M T$ versus T curves, the increase of the $\chi_M T$ values with decreasing temperature and the higher room temperature $\chi_M T$ values than the corresponding expected spin-only values reveal the presence of dominant ferromagnetic exchange interactions in both compounds. The maximum $\chi_M T$ value at 10 K reveals that **1**·6H_2O possesses a ground-state spin value of $S = 23/2$ or 21/2; the spin-only ($g = 2$) values for $S = 23/2$ and 21/2 ground states are 71.88 and 60.38 cm^3 mol^{-1} K, respectively. For compound **2**, the $\chi_M T$ near-plateau value in the 20–40 K range appears to be heading for a final value of ~79 cm^3 mol^{-1} K which is very close to the spin-only ($g = 2$) value of a species with an S = 12 ground state (78 cm^3 mol^{-1} K), the maximum possible S_T value for a complex containing 6 Mn^{III} ions, indicating that it exhibits entirely ferromagnetic exchange interactions. The low temperature decrease appearing in the $\chi_M T$ versus T plots of **1**·6H_2O and **2** is due to Zeeman effects, zero-field splitting and/or weak intermolecular interactions.

The dc magnetic susceptibility data for **2** were fit to the theoretical $\chi_M T$ versus T expression derived from the spin Hamiltonian appropriate for a $[Mn^{III}_6]$ octahedron (see discussion of the crystal structure of **2** and Fig. 3, bottom, right); given in Eq. (3),

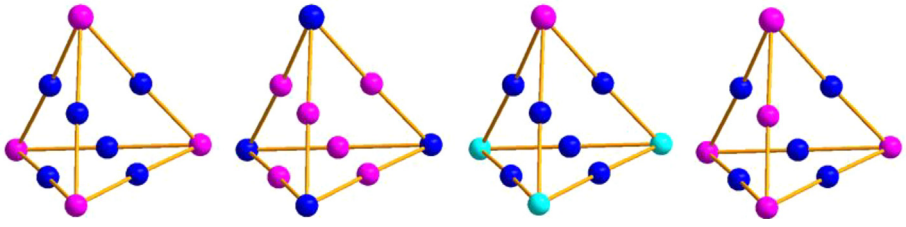

Fig. 4. The Mn/M (M = heterometal) ions distribution in complex **1** (left) and those of reported heterometallic $[Mn_{10-x}M_x]$ supertetrahedra.[24,27–30] From left to right the metallic skeletons of $[Mn^{III}_6Ca^{II}_4]$, $[Mn^{III}_4Ce^{IV}_6]$, [27] $[Mn^{III}_6Mn^{II}_3M]$ (M = M = Na^+, Sr^{2+}, Cd^{2+}, Y^{3+}, Dy^{3+}, Lu^{3+}) [24,29,30] and $[Mn^{III}_5Dy^{III}_5]$ [28] heterometallic decametallic supertetrahedra are shown. Colour code: Mn^{III}, blue; Mn^{II}, cyan, Heterometal, purple. (Colour online.)

$$\hat{H} = -2J_{cis}(\hat{S}_1 \cdot \hat{S}_2 + \hat{S}_1 \cdot \hat{S}_3 + \hat{S}_1 \cdot \hat{S}_4 + \hat{S}_1 \cdot \hat{S}_6 + \hat{S}_2 \cdot \hat{S}_3 + \hat{S}_2 \cdot \hat{S}_5 + \hat{S}_2 \cdot \hat{S}_6 + \hat{S}_3 \cdot \hat{S}_4 + \hat{S}_3 \cdot \hat{S}_5 + \hat{S}_4 \cdot \hat{S}_5 + \hat{S}_4 \cdot \hat{S}_6 + \hat{S}_5 \cdot \hat{S}_6) - 2J_{trans}(\hat{S}_1 \cdot \hat{S}_5 + \hat{S}_2 \cdot \hat{S}_4 + \hat{S}_3 \cdot \hat{S}_6) \quad (3)$$

where S_i refers to the spin of metal ion Mn_i ($S_1 = S_2 = S_3 = S_4 = S_5 = S_6 = 2$), and J_{cis} and J_{trans} are the pairwise exchange parameters for metal ions located in neighboring and opposite positions of the octahedron, respectively; the labeling scheme employed for the Mn ions of the Mn_6^{III} octahedron of **2** is shown in Fig. S1 in the Supplementary information. The eigenvalues of Eq. (3) are given in Eq. (4), where $\hat{S}_A = \hat{S}_1 + \hat{S}_5$, $\hat{S}_B = \hat{S}_2 + \hat{S}_4$, $\hat{S}_C = \hat{S}_3 + \hat{S}_6$, and $\hat{S}_T = \hat{S}_A + \hat{S}_B + \hat{S}_C$; S_T is the resultant spin of the complete molecule:

$$E(S_T) = -J_{cis}[S_T(S_T+1) - S_A(S_A+1) - S_B(S_B+1) - S_C(S_C+1)] - J_{trans}[S_A(S_A+1) + S_B(S_B+1) + S_C(S_C+1)] \quad (4)$$

We note that constant terms contributing equally to all states have been omitted from Eq. (4). An expression for the molar paramagnetic susceptibility, χ_M, was derived using the above and the Van Vleck equation, and assuming an isotropic g tensor. The derived equation was then used to fit the experimental $\chi_M T$ versus T data in Fig. 5 as a function of the two exchange parameters J_{cis} and J_{trans}, and the g factor. Only data for the 20–300 K range were used, since the model does not incorporate ZFS and other minor effects appearing at lower temperatures. A good quality fit was obtained (represented from the solid line of Fig. 5) with fit parameters of $J_{cis} = 3.8 \pm 0.2$ cm^{-1}, $J_{trans} = 1.2 \pm 0.8$ cm^{-1}, and $g = 2.02 \pm 0.002$, with temperature independent paramagnetism (TIP) held constant at 600×10^{-6} cm^3 mol^{-1}. The fit indicates that [$Mn_6^{III}Ca_4^{II}$] complex has an $S_T = 12$ ground state. In the notation $|S_T, S_A, S_B, S_C|$ this is the |12, 4, 4, 4| state in which all six Mn^{III} spins are aligned parallel. The first excited state is a triply degenerate set of $S_T = 11$ states comprising the |11, 3, 4, 4|, |11, 4, 3, 4|, and |11, 4, 4, 3| states at 366 cm^{-1} above the ground state. Thus, the S = 12 ground state is well isolated from the nearest excited state.

Given the size of the [Mn_{10}] cluster of **1**·6H_2O, and the resulting number of inequivalent exchange constants, it was not possible to apply the Kambe method to determine the individual pairwise Mn_2 exchange interaction parameters. We concentrated instead on obtaining additional information for the ground-state spin, S_T, and the zero-field splitting parameter, D, of **1**·6H_2O and **2** by performing magnetization versus dc field measurements at applied magnetic fields and temperatures in the 1–70 kG and 1.8–10 K ranges, respectively. The data for complex **1**·6H_2O and **2** are shown in Fig. 6 as reduced magnetization ($M/N\mu_B$) versus H/T plots, where M is the magnetization, N is Avogadro's number, μ_B is the Bohr magneton, and H is the magnetic field. The $M/N\mu_B$ versus H/T data were fit using the program MAGNET to a model that assumes that only the ground state is populated at these temperatures and magnetic fields, includes isotropic Zeeman interactions and axial zero-field splitting ($D\hat{S}_z^2$), and incorporates a full powder average. The corresponding spin Hamiltonian is given by Eq. (5),

$$H = D\hat{S}_z^2 + g\mu_B\mu_0\hat{S} \cdot H \quad (5)$$

where D is the axial ZFS parameter, $\hat{S}_z$ is the easy-axis spin operator, μ_0 is the vacuum permeability, and H is the applied field. The last term in Eq. (5) is the Zeeman energy associated with an applied magnetic field. The variable-field variable-temperature magnetization data for **1**·6H_2O were fitted when low field data, up to 1 T, were used to minimize problems arising from the presence of low-lying excited states as has been reported for other high nuclearity Mn clusters. [24–26] The best fit for **1** is shown as the solid lines in Fig. 6, top and was obtained with $S = 23/2$, $g = 1.94$, and $D = -0.048$ cm^{-1}. Alternative fits with $S = 21/2$ and 25/2 were also

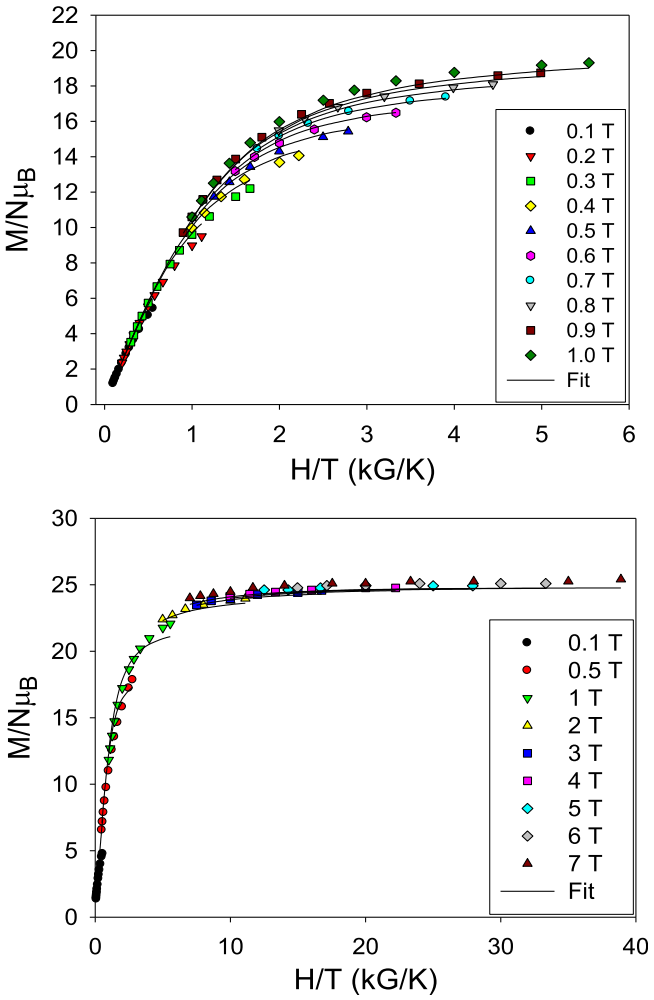

Fig. 6. Plots of reduced magnetization ($M/N\mu_B$) *vs* H/T for complexes **1**·6H_2O (top) and **2** (bottom) at the indicated fields and in the 1.8–10 K temperature range. The solid lines are the fit of the data; see the text for the fit parameters.

achieved with fit parameters $g = 2.04$ and $D = -0.053$ cm^{-1} and $g = 1.93$ and $D = -0.062$ cm^{-1}, respectively. The different possible fits of the magnetization data are assigned to the large number of low-lying excited states which is a general property in high nuclearity Mn clusters with high S values. [24,25] For complex **2**, a satisfactory fit was obtained using all data up to 7 T. This indicates that its ground state is relatively well-isolated from the nearest excited states, as suggested from the obtained fit of the variable temperature magnetic susceptibility data (vide supra). The best fit shown as the solid lines in the reduced magnetization ($M/N\mu_B$ versus H/T) plot in Fig. 6, bottom was obtained with $S = 12$, $g = 2.07$, and $D = -0.051$ cm^{-1}. It is recognized that the g value is too high, however this fit is a rough estimate mainly for the S and D values of the compound which in this case are realistic. Note that the D values determined for **1** and **2** are very small being in line with the reported D values of known Mn supertetrahedra [11–14,16,20]. More accurate information for the g values could be obtained using other techniques; such investigations however, are beyond the scope of this paper.

Ac magnetic susceptibility studies at zero dc field and 3.5 G ac field were also carried out. Ac susceptibility studies are a powerful complement to dc studies for determining the ground state of a system, because they remove the complications arising from the presence of a dc field. The obtained in-phase χ'_M signal for

complexes **1**·6H_2O and **2** are plotted as χ'_MT versus T in Figs. S2 and S3 in the Supplementary information. The χ'_MT value for **1**·6H_2O increases with decreasing temperature from 15 K to 10 K and then it remains stable before it decreases at ~5 K. Extrapolation of the χ'_MT data from the plateau (~6–9 K) to 0 K, at which point only the ground state will be populated, gives a value of ~70 cm^3 mol^{-1} K consistent with an S = 23/2 assuming a g value slightly less than two. Thus, based on the conclusions arising from the various types of dc and ac magnetic measurements it is suggested that complex **1** exhibits a spin ground state value S_T = 23/2. The χ'_MT value for **2** decreases slightly from 15–5 K as expected for a compound exhibiting a well-isolated ground state and then more rapidly below 5 K. Extrapolation of the χ'_MT versus T plot from T > 6 K to avoid phenomena appearing at lower temperatures gives a value of ~78 cm^3 mol^{-1} K, which is consistent with an S = 12 ground state, in excellent agreement with the findings from variable-field variable-temperature magnetization and variable temperature magnetic susceptibility studies. We thus conclude that complex **2** does have an S_T = 12 ground state. Finally, complexes **1** and **2** do not exhibit any out-of-phase ac magnetic susceptibility signals down to 1.8 K.

4. Conclusions

The initial use of triol btH_3 in Mn carboxylate chemistry and the extension of our investigations on the employment of pdH_2 on the synthesis of mixed metal Mn/M clusters afforded a homometallic $Mn^{III}_9Mn^{II}$ cluster and a heterometallic $Mn^{III}_6Ca^{II}_4$ aggregate. Compounds **1** and **2** exhibit $[Mn^{III}_9Mn^{II}(\mu_4\text{-}O)_4]^{21+}$ and $[Mn^{III}_6Ca^{II}_4(\mu_4\text{-}O)_4]^{18+}$ supertetrahedral structural cores, respectively being members of an extended family of metal complexes combining high symmetry crystal structures and interesting magnetic properties. In particular Mn supertetrahedra often display ferromagnetic exchange interactions and the maximum possible spin ground state values. In fact this family includes members displaying giant S_T values such as 83/2, [6] 37, [7] 61/2, [24] 26 [25] and 22 [12–14,16,17]. Interestingly, complex **1** displays a $Mn^{III}_9Mn^{II}$ oxidation state level that appears for the first time in the rich family of homometallic $[Mn_{10}]$ supertetrahedra. In addition, complex **2** displays a core related to the common $[Mn^{III}_6Mn^{II}_4(\mu_4\text{-}O)_4]^{18+}$ supertetrahedral one in which the four Mn^{II} ions are replaced by Ca^{II} ions. This heterometal ion distribution has not appeared again in any mixed metal $[Mn_{10-x}M_x]$ (M = any metal ion) cluster. Dc and ac magnetism studies revealed that **1** and **2** display dominant and entirely ferromagnetic exchange interactions leading to S_T values 23/2 and 12, respectively.

The isolation of complex **1** establishes the potential of the unexplored coordination chemistry of the triol btH_3 to become a rich source of new compounds with novel crystal structures and interesting magnetism. In addition, the formation of the two supertetrahedral compounds **1** and **2** further demonstrates the capability of polyol-type ligands to stabilize various types of supertetrahedra appearing either in discrete form or as fragments of high nuclearity metal clusters. Although there have been quite a few studies in this area, additional investigations will definitely afford new types of molecular superetetrahedral aggregates exhibiting interesting properties. Further synthetic efforts involving the detailed exploration of the use of polyols, including btH_3, in Mn and mixed metal Mn/M cluster chemistry are currently in progress.

Acknowledgement

This work was supported by a University of Cyprus internal research grant.

Appendix A. Supplementary data

CCDC 1831777 and 1831778 contains the supplementary crystallographic data for compounds **1**·3H_2O and **2**, respectively. These data can be obtained free of charge via http://www.ccdc.cam.ac.uk/conts/retrieving.html, or from the Cambridge Crystallographic Data Centre, 12 Union Road, Cambridge CB2 1EZ, UK; fax: (+44) 1223-336-033; or e-mail: deposit@ccdc.cam.ac.uk.

Supplementary data (various structural and magnetism figures) associated with this article can be found, in the online version, at https://doi.org/10.1016/j.poly.2018.05.029.

References

[1] C. Papatriantafyllopoulou, E.E. Moushi, G. Christou, A.J. Tasiopoulos, Chem. Soc. Rev. 45 (2016) 1597.
[2] J. Fernando-Soria, J. Vallejo, M. Castellano, J. Martinez-Lillo, E. Pardo, J. Cano, I. Castro, F. Lloret, R. Ruiz-García, M. Julve, Coord. Chem. Rev. 339 (2017) 17.
[3] R. Bagai, G. Christou, Chem. Soc. Rev. 38 (2009) 1011.
[4] C.J. Milios, R.E.P. Winpenny, Struct. Bonding 164 (2015) 1.
[5] S. Kang, H. Zheng, T. Liu, K. Hamachi, S. Kanegawa, K. Sugimoto, Y. Shiota, S. Hayami, M. Mito, T. Nakamura, M. Nakano, M.L. Baker, H. Nojiri, K. Yoshizawa, C. Duna, O. Sato, Nat. Commun. 6 (2015) 5955.
[6] A.M. Ako, I.J. Hewitt, V. Mereacre, R. Clérac, W. Wernsdorfer, C.E. Anson, A.K. Powell, Angew. Chem. Int. Ed. 45 (2006) 4926.
[7] E.E. Moushi, T.C. Stamatatos, W. Wernsdorfer, V. Nastopoulos, G. Christou, A.J. Tasiopoulos, Inorg. Chem. 48 (2009) 5049.
[8] Y.-Z. Zheng, G.-J. Zhou, Z. Zheng, R.E.P. Winpenny, Chem. Soc. Rev. 43 (2014) 1462.
[9] A. Escuer, J. Esteban, S.P. Perlepes, T.C. Stamatatos, Coord. Chem. Rev. 275 (2014) 87.
[10] A.J. Tasiopoulos, S.P. Perlepes, Dalton Trans. (2008) 5537.
[11] M. Manoli, R.D.L. Johnstone, S. Parsons, M. Murrie, M. Affronte, M. Evangelisti, E.K. Brechin, Angew. Chem. Int. Ed. 46 (2007) 4456.
[12] M. Manoli, A. Collins, S. Parsons, A. Candini, M. Evangelisti, E.K. Brechin, J. Am. Chem. Soc. 130 (2008) 11129.
[13] T.C. Stamatatos, K.A. Abboud, W. Wernsdorfer, G. Christou, Angew. Chem. Int. Ed. 45 (2006) 4134.
[14] T.C. Stamatatos, K.M. Poole, K.A. Abboud, W. Wernsdorfer, T.A. O'Brlen, G. Christou, Inorg. Chem. 47 (2008) 5006.
[15] J. Utko, A.B. Canaj, C.J. Milios, M. Sobocińska, T. Lis, Inorg. Chem. Commun. 45 (2014) 71.
[16] G. Wu, J. Huang, L. Sun, J. Bai, G. Li, E. Cremades, E. Ruiz, R. Clérac, S. Qiu, Inorg. Chem. 50 (2011) 8580.
[17] S. Nayak, M. Evangelisti, A.K. Powell, J. Reedijk, Chem. Eur. J. 16 (2010) 12865.
[18] S.M. Taylor, R.D. Mclntosh, J. Rezé, S.J. Dalgarno, E.K. Brechin, Chem. Commun. 48 (2012) 9263.
[19] D.P. Goldberg, A. Caneschi, S.J. Lippard, J. Am. Chem. Soc. 115 (1993) 9299.
[20] D.P. Goldberg, A. Caneschi, C.D. Delfs, R. Sessoli, S.J. Lippard, J. Am. Chem. Soc. 117 (1995) 5789.
[21] L.F. Jones, G. Rajaraman, J. Brockman, M. Murugesu, E.C. Sañudo, J. Raftery, S.J. Teat, W. Wernsdorfer, G. Christou, E.K. Brechin, D. Collison, Chem. Eur. J. 10 (2004) 5180.
[22] S. Nayak, L.M.C. Beltran, Y. Lan, R. Clérac, N.G.R. Hearns, W. Wernsdorfer, C.E. Anson, A.K. Powell, Dalton Trans. (2009) 1901.
[23] E.E. Moushi, T.C. Stamatatos, V. Nastopoulos, G. Christou, A.J. Tasiopoulos, Polyhedron 28 (2009) 1814.
[24] M. Manoli, S. Alexandrou, L. Pham, G. Lorusso, W. Wernsdorfer, M. Evangelisti, G. Christou, A.J. Tasiopoulos, Angew. Chem. Int. Ed. 55 (2016) 679.
[25] M. Charalambous, E.E. Moushi, C. Papatriantafyllopoulou, W. Wernsdorfer, V. Nastopoulos, G. Christou, A.J. Tasiopoulos, Chem. Commun. 48 (2012) 5410.
[26] E.E. Moushi, A. Masello, W. Wernsdorfer, V. Nastopoulos, G. Christou, A.J. Tasiopoulos, Dalton Trans. 39 (2010) 4978.
[27] V. Mereacre, A.M. Ako, M.N. Akhtar, A. Lindemann, C.F. Anson, A.K. Powell, Helv. Chim. Acta 92 (2009) 2507.
[28] S.K. Langley, B. Moubaraki, K.S. Murray, Dalton Trans. 39 (2010) 5066.
[29] A.M. Ako, V. Mereacre, R. Clérac, W. Wernsdorfer, I.J. Hewitt, C.E. Anson, A.K. Powell, Chem. Commun. (2009) 544.
[30] A.M. Ako, B. Burger, Y. Lan, V. Mereacre, R. Clérac, G. Buth, S. Gomez-Coca, E. Ruiz, C.E. Anson, A.K. Powell, Inorg. Chem. 52 (2013) 5764.
[31] J.B. Vincent, H.-R. Chang, K. Folting, J.C. Huffman, G. Christou, D.N. Hendrickson, J. Am. Chem. Soc. 109 (1987) 5703.
[32] Oxford Diffraction 2008, CrysAlis CCD and CrysAlis RED, Version 1.171.32.15, Oxford Diffraction Ltd., Abingdon, Oxford, England.
[33] A. Altomare, M.C. Burla, M. Camalli, G. Cascarano, C. Giacovazzo, A. Guagliardi, G. Polidori, J. Appl. Crystallogr. 27 (1994) 435.
[34] G.M. Sheldrick, SHELXL-97, Program for Refinement of Crystal Structures, University of Göttingen, Germany, 1997.
[35] P. Van der Sluis, A.L. Spek, Acta Crystallogr., Sect. A: Found Crystallogr. A46 (1990) 194.
[36] L.J. Farrugia, J. Appl. Crystallogr. 32 (1999) 837.

[37] K. Brandenburg, DIAMOND, Version 2003.2001d, Crystal Impact GbR, Bonn, Germany, 2006.
[38] S. Zartilas, C. Papatriantafyllopoulou, T.C. Stamatatos, V. Nastopoulos, E. Cremades, E. Ruiz, G. Christou, C. Lampropoulos, A.J. Tasiopoulos, Inorg. Chem. 52 (2013) 12070.
[39] M. Charalampous, S.M. Zartilas, E.E. Moushi, C. Papatriantafyllopoulou, M.J. Manos, T.C. Stamatatos, S. Mukherjee, V. Nastopoulos, G. Christou, A.J. Tasiopoulos, Chem. Commun. 50 (2014) 9090.
[40] E.E. Moushi, T.C. Stamatatos, W. Wernsdorfer, V. Nastopoulos, G. Christou, A.J. Tasiopoulos, Angew. Chem. Int. Ed. 45 (2006) 7722.
[41] E.E. Moushi, C. Lampropoulos, W. Wernsdorfer, V. Nastopoulos, G. Christou, A.J. Tasiopoulos, Inorg. Chem. 46 (2007) 3795.
[42] S. Mukherjee, J.A. Stull, J. Yano, T.C. Stamatatos, K. Pringouri, T.A. Stich, K.A. Abboud, R.D. Britt, V.K. Yachandra, G. Christou, PNAS 109 (2012) 2257.
[43] W. Liu, H.H. Thorp, Inorg. Chem 32 (1993) 4102.
[44] I.D. Brown, D. Altermatt, Acta Crystallogr. B41 (1985) 244.